Journal of Energy Storage 97 (2024) 112917

Contents lists available at ScienceDirect

Journal of Energy Storage

journal homepage: www.elsevier.com/locate/est

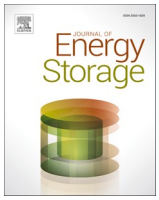

Research papers

Electromagnetic, cooling, and strain-based multi-objective optimization of superconducting magnetic energy storage unit for power grid applications

Alireza Sadeghi [a], Antonio Morandi [b], Mohammad Yazdani-Asrami [a,*]

[a] CryoElectric Research Lab, Propulsion, Electrification & Superconductivity Group, James Watt School of Engineering, University of Glasgow, Glasgow G12 8QQ, United Kingdom

[b] Department of Electrical, Electronic, and Information Engineering, University of Bologna, Viale del Risorgimento 2, 40136 Bologna, Italy

ARTICLE INFO

Keywords:
NSGA II
Loading factor
Energy density
Strain
Cost
Weight
Objective function
Pareto front

ABSTRACT

Based on the requirements of microgrids and Uninterruptible Power Supply systems, an MJ-class energy storage device is necessary to enhance the stability of microgrids during power interruptions and outages. This study focuses on optimizing the design routines of an MJ-class Superconducting Magnetic Energy Storage (SMES) unit using an intelligent optimization method known as Non-dominated Sorting Genetic Algorithm II. SMES units are among the potential storage devices for future power systems. However, due to their cooling cost, weight, and energy density, they have not yet been commercialized for power system applications. In this regard, this study discusses the impact of considering mechanical, economic, magnetoelectric, and physical objective functions during the design optimization of MJ-class SMES, as novel design functions for SMES units. The following objective functions were employed: maximization of energy density, minimization of total weight, minimization of total cooling cost, and minimization of maximum applied strain. Different loading factors were also analyzed to demonstrate their importance in the final design of SMES. This has been conducted to show how loading factor could change the final design of the SMES units. Here, loading factor is considered as the ratio of operational current to the critical current of the high temperature superconducting tapes. Results indicate that considering all the objective functions during the optimization process of SMES leads to a more realistic final design, presenting an SMES unit with a feasible structure for operation and manufacturing. Additionally, the increase in loading factor was found to reduce the heat load, increase the maximum applied strain, and raise the weight of the SMES. This underscores the significance of considering this parameter during the design process of SMES. Finally, the results of analytical model used for design of SMES have been compared with finite element results to validate the model used in this study.

1. Introduction

Due to uncertain nature of input energy of Renewable Energy Resources (RERs) such as wind farms and photovoltaic units, the power system connected to RERs could end up with frequency oscillation and instability, curtailment of renewable generation, invasive load shedding and low voltage quality [1]. Energy storage units are technologies that have been offered to address the stability and reliability issues of power systems with high penetration level of RERs. Energy storage units improve the frequency regulation, integrate the spinning reserve in power system and improve the peak management programs in power systems [2]. Among existing storage units, such as batteries, pumped hydroelectric storage units, and thermal energy storage units, Superconducting Magnetic Energy Storage (SMES) units offer a wide range of benefits over other technologies such as fast response time, high level of delivered power, and virtually infinite number of charge/discharge cycles with no degradation [3–8]. These characteristics have increased interests in using SMES units for applications such as microgrids, stand-alone grids, and power systems with RERs [9].

Although SMES units offer wide range of advantages, their application for MJ-classes faces challenges such as low energy density, persistent need of cooling power, high stand-by losses in power electronic components, and high level of strain and Lorentz forces for high energy coils. Recently, investigations were performed to optimize the structure of SMES units and deal with the challenges [10–13]. Reference [14] is one of the first papers dealing with SMES optimization, though, no

* Corresponding author.
E-mail address: mohammad.yazdani-asrami@glasgow.ac.uk (M. Yazdani-Asrami).

https://doi.org/10.1016/j.est.2024.112917
Received 8 February 2024; Received in revised form 6 June 2024; Accepted 8 July 2024
Available online 17 July 2024

mechanical aspects were considered in this reference. In [15], a mathematical-based optimization was used for a 5 MJ High Temperature Superconducting (HTS) SMES to maximize the specific energy of the HTS coil. In [16], the use of analytical functions interpolating numerical data was proposed to carry out fast optimization of SMEs systems. In [17–19], an evolutionary algorithm was used to minimize the coil volume of a 1 MJ class SMES. In [20,21], a combination of finite element method and evolutionary algorithms were used to maximize the energy density of an SMES unit while the structure of coils have been changed. A 0.5 MJ SMES coil was designed in [22] based on volume minimization of coil and maximizing its inductance and current capacity. Although studies were conducted on design optimization of SMES units, most of them were concentrated on Alternative Current (AC) loss issues [23–25], cost of HTS wires, and sometimes energy density of SMES units. Recently, efforts have been elaborated to simultaneously optimize the design of the SMES units, regarding their physical and electrical constraints [26–28]. In [29], design optimization of an SMES unit has been conducted that aims to minimize the volume of the solenoid while the magnetic field homogeneity inside the coil is to be maximized. In [30], a control strategy is proposed for an SMES unit based on a multi-objective genetic algorithm that aims to damp the frequency oscillations and steady-state error after any change in the demanded load. In [31] a multi-objective design study has been performed aimed to maximize the magnetic field uniformity inside the coil, minimize the volume of the coil, and minimize the stress imposed on the superconducting coil. Another study presented a compactness-efficiency optimization function that is solved through simulated annealing method [32]. As can be seen, the trend is to use multi-objective design procedures for designing the HTS SMES units that could satisfy the needs of the power systems in high energy range. However, in this regard, there is a gap to optimally design the HTS SMES units with respect to physical, electrical, magnetic, cooling system, economic, and mechanical considerations. These considerations are critically important during the design process of the SMES units, since the electromagnetic considerations could ensure the proper amount of energy delivered to the grid, mechanical consideration should be studied to reduce the possibility of quenches. Thermal and cooling considerations are important due to their direct impact on the efficiency of the SMES, and finally economic considerations are always significant objectives in world of engineering.

In this paper, a multi-objective design optimization is performed by taking energy density, weight, cooling cost, and maximum allowable strain into the consideration of SMES designing procedure. The aim of this optimization study is to maximize the gravimetric energy density (with respect to the conductor only. In other words, this could be minimizing the usage of conductor), minimize the weight, cooling cost, and the applied strain to HTS tapes of an SMES unit. Non-dominated Sorting Genetic Algorithm II (NSGA II) was used for finding the feasible solutions for such optimization problem. The optimization variables are number of pancake coils, number of turns, coil inner radius, distance between turns, and distance between pancake coils that are subject to inequality constraints. For instance, the inner radius of the pancakes cannot be lower than the minimum bending radius of the tape. Optimization process was performed for different ratio of operating current to critical current (loading factor m), from 0.2 to 1. Although the practical range of loading factor during the design of SMES devices is between 0.5 and 0.8, the 0.2 to 1 range is selected to characterize the behavior SMES and HTS coil in a wider range to show the trends. In fact, loading factor is not really a degree of freedom during design procedure of SMES and it represents more of a safety margin. The higher the load factor, the higher the risk during quenching. A sound motivated choice of the loading factor can only be obtained from quench analysis beyond this paper's scope. Firstly, the model is validated by comparing the results with those reported in literature. Then, the results of the multi objective optimization are compared with the results of single objective optimization to show how energy density, wire length, etc. are changed to take other objectives into account so to make the design feasible. After that, results show the importance of considering a sensible loading factor during design optimization.

2. Proposed SMES design functions, constraints, and equations

As shown in Fig. 1, any SMES unit consists of the AC to Direct Current (DC) power converter, control unit of converter, superconducting coils, cryostat, and the refrigeration system. The current flows from upstream power grid into the AC/DC inverter which is controlled by control unit. Then, AC power is converted into DC power and the DC current induces magnetic field in the HTS coil which is considered here as pancake coil. As a matter of fact, SMES stores electrical energy in the form of magnetic field in the coil inductance and by discharging the coil, the stored energy could flow back to the grid.

Suppose that the understudied SMES in Fig. 1, consists of four HTS Pancake Coils (PCs) with an inner radius of (R_{in}), as shown in Fig. 2. Also, the distance between PCs is (dp) and each Pancake Coils (PC) has N_t turns with a (dt) distance between turns. The outer radius (R_{out}) and height (h) of the HTS coil is calculated based on Eqs. (1) and (2) [33].

$$h = (N_p - 1)dp + w_{tape}N_p \tag{1}$$

$$R_{out} = R_{in} + (N_t - 1)dt + N_t\delta_{tape} \tag{2}$$

where, N_p is number of PCs, w_{tape} is width of HTS tape and δ_{tape} is thickness of HTS tape.

Then, the maximum magnetic field of the coil (B_{max}) is calculated based on Eq. (3) [33].

$$B_{max} = \frac{0.5\mu_0 N_t N_p I_{op}}{((N_t - 1)dt + \delta_{tape})} ln\left(\frac{\frac{R_{out}}{R_{in}} + \sqrt{\left(\frac{R_{out}}{R_{in}}\right)^2 + \left(\frac{h}{2R_{in}}\right)^2}}{1 + \sqrt{1 + \left(\frac{h}{2R_{in}}\right)^2}}\right) \tag{3}$$

where, μ_0 is relative permeability of vacuum equal to $1.257 \times 10^{-6}\frac{H}{m}$ and I_{op} is operating current in (A) which is considered as a function of critical current (I_c) and loading factor (m) i.e. $I_{op} = m \times I_c$.

The critical current must be considered magnetic field dependent which is formulated as Eq. (4) [33]:

$$I_c(B_{max}, B_{ze}, B_{re}) = \frac{I_{c0}}{\left(1 + \left(c_1 B_{max}\sqrt{\left(c_2\frac{B_{ze}}{B_m}\right)^2 + \left(\frac{B_{re}}{B_m}\right)^2}\right)\right)^{c_3}} \tag{4}$$

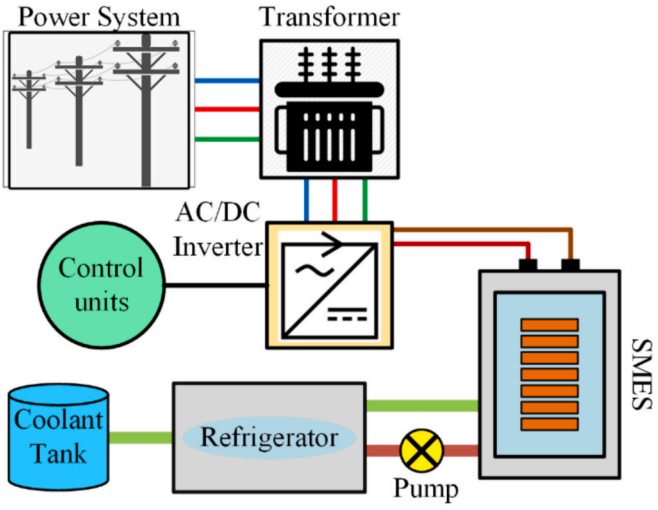

Fig. 1. The simple schematic of a typical SMES unit and its components.

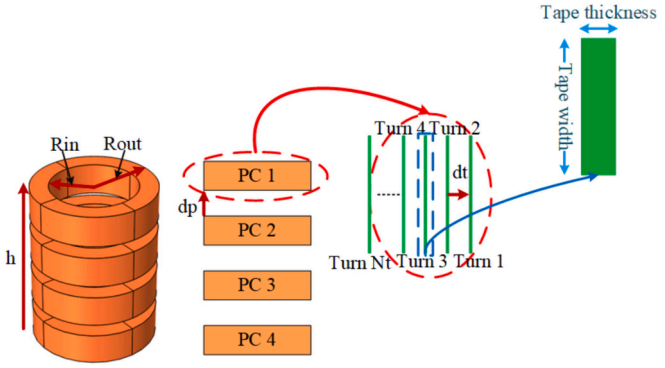

Fig. 2. Superconducting coil structure in an SMES consisting of four PCs.

where, I_{c0} is critical current at self-field, B_{ze} and B_{re} are azimuthal and radial magnetic fields at top and bottom end of the coil that are calculated according to [34].

The weight of the coil's conductor (W_{coil}) is calculated according to Eq. (5) in kilograms, and the total length of HTS tapes (L_w) used in the SMES coil is calculated using equation in meters (6) [35].

$$W_{coil} = \pi \times h \times \left(R_{out}^2 - R_{in}^2\right) \times D_{tape} \tag{5}$$

$$L_w = \frac{2\pi \times \left(\frac{N_p N_t I_{op}}{J_{tape} h (R_{out} - R_{in})}\right) \times \left(R_{in} + \frac{R_{out} - R_{in}}{2}\right) \times h \times \left(\frac{R_{out} - R_{in}}{2}\right)}{w_{tape} \times \delta_{tape}} \tag{6}$$

where, D_{tape} is density of HTS tape in kg/m^3, J_{tape} is current density of HTS tape, and w_{tape} is width of HTS tape.

Then, inductance (L_{coil}), energy (E_{coil}), and volumetric energy density (ED) of the SMES is calculated based on Eqs. (7) to (9) [33,36]:

$$L_{coil} = \frac{\mu_0 \pi \left(N_t N_p\right)^2 A}{h} \times \frac{1}{1 + 0.9\left(\frac{R_{in}}{h} + \frac{R_{out} - R_{in}}{2h}\right) + 0.64\left(\frac{R_{out} - R_{in}}{R_{out} + R_{in}}\right) + 0.84\left(\frac{R_{out} - R_{in}}{h}\right)} \tag{7}$$

$$E_{coil} = \frac{1}{2} L_{coil} I_{op}^2 \tag{8}$$

$$ED = \frac{E_{coil}}{V_{coil}} = \frac{E_{coil}}{\pi \times h \times \left(R_{out}^2 - R_{in}^2\right)} \tag{9}$$

where coefficient A is equal to $A = \pi\left(R_{in} + \frac{R_{out} - R_{in}}{2}\right)^2$.

The next step is to calculate the heat load, in Watt, imposed to the cooling system that includes heat load by current leads $\left(\dot{Q_{lead}}\right)$, resistive heat load $(\dot{Q_R})$, and radiation heat load $\left(\dot{Q_{rad}}\right)$ that are calculated based on Eqs. (10) to (12) [37].

$$\dot{Q_{lead}} = 4\, I_{op} \sqrt{100 \times \rho_{cu} \times \left(T_{amb} - T_{op}\right)} \tag{10}$$

$$\dot{Q_R} = 10^{-4} I_{op} L_w^{n(B)} \tag{11}$$

$$\dot{Q_{rad}} = \dot{q_{rad}} \times 2\pi \times R_{out} \tag{12}$$

where, ρ_{cu} is resistivity of copper at room temperature $\left(1.68 \times 10^{-8}\ \Omega.m\right)$, T_{amb} is ambient temperature, i.e., 300 K, T_{op} is operating temperature, as the minimum allowable temperature for cryocooler, $n(B)$ is magnetic field dependent index value, and $\dot{q_{rad}}$ is radiation heat flux considered to be 3 $\frac{W}{m^2}$ [38].

Demanded cooling power (P_{cool}) by SMES, in W, is calculated by Eq. (13) [37], and Eq. (14) calculates the purchasing cost, in British Sterling Pound, of providing such cooling power (C_{cool}) at 20 K operating temperature [39].

$$P_{cool} = 1.1 \dot{Q_{total}} \left(\frac{T_{amb} - T_{op}}{T_{op}}\right) \times \left(\frac{1}{-3.5335 \times 10^{-9} T_{op}^3 - 9.9354 \times 10^{-6} T_{op}^2 + 3.2995 \times 10^{-3} T_{op}}\right) \tag{13}$$

$$C_{cool}(GBP) = 7.53 \times P_{cool}^{0.412} \tag{14}$$

At last, the maximum applied stress $(\sigma_{\max})$, in N/m^2, to HTS tapes is calculated based on Eqs. (15) and (16) [35]:

$$\sigma_{\max} = J_{tape} B_{max} R_{in} \times \left(\frac{1}{r-1}\right) \times \left[\frac{2r(7r^2 + r + 1)}{9(r+1)} - \frac{5}{12}\left(2r^2 + r - 0.6\right)\right] \tag{15}$$

$$r = 1 + \frac{2(R_{out} - R_{in})}{R_{in}} \tag{16}$$

If stress is not considered during SMES design procedure, we may have an SMES unit with the highest possible energy density, lowest cooling cost and weight. Then, suddenly when it is energized, the HTS tapes would quench driven by stress and transit into the non-superconducting state and make the design impractical.

3. An overview on the NSGA II optimization method

A Multi-Objective Optimization (MOO) problem deals with finding a series of optimum solutions for multiple objective functions which are considered all together simultaneously, while a Single Objective Optimization (SOO) problem concerns with just one objective function. A general MOO problem subjected to a feasible domain is shown in Eq. (17) [40,41].

$$\begin{gathered} min\ \left\{f_1(x_1, x_2, \ldots, x_n), f_2(x_1, x_2, \ldots, x_n), \ldots, f_p(x_1, x_2, \ldots, x_{n_v})\right\}\ p \geq 2 \\ subject\ to\ x_i \in U \end{gathered} \tag{17}$$

where, p is number of objective functions, n_v is the number of decision variables, U is the feasible set, x_i is i^{th} decision variable, and $f_p(x_1, x_2, \ldots, x_{n_v})$ is the p^{th} objective function.

Unlike SOO problem, every MOO problem offers a p–dimensional space related to objective functions that is mapped by a vector of decision variables, as shown in Fig. 3 which is a simple illustration for a MOO with two objective functions and two decision variables.

As said before, the solution for every MOO problem is a group of p-dimensional solutions, known as feasible front. One of the most significant methods to find optimum front is known as Pareto front which works based on the "dominance" [42]. In the Pareto method and during

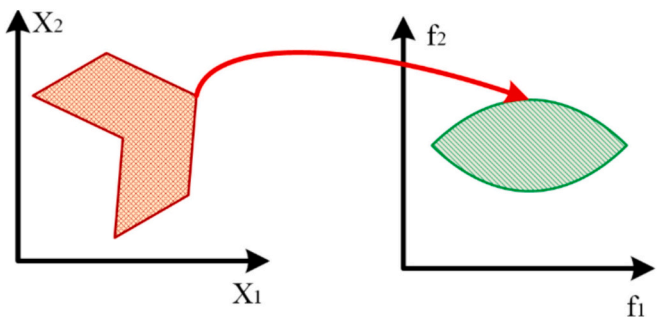

Fig. 3. Mapping the vector of decision variables into 2D space of objective functions, dedicated for a MOO problem.

optimization, the optimum solutions are independent from each other. Meanwhile, with respect to domination rules, all the solutions will be categorized into two subclasses, dominated and non-dominated. The first term refers to those solutions where one objective function may not increase without the chance of reducing the other objective function. The final dominated solutions are also called Pareto front. The non-dominated solutions are also defined as those solutions where one objective function could be improved without any need to reduce/worsen other objective functions [43].

One of the most famous methods to gain the Pareto front of MOO problems is known as NSGA-II which was firstly proposed by Deb et al. [44] to solve the optimization problems with more than one objective functions. In this algorithm, four rules are considered to reach a feasible vector of results, Pareto front that are non-dominated sorting, elite preserving operator, crowding distance, and selection operator [40]. Initially, for a random and non-dominated population, each objective function is calculated. Afterwards, everyone is sorted into the non-domination levels which is conducted by non-dominated method. The next step is to sort the individuals with same level of domination based on crowding distance method and then, a crossover function is applied that offers two parents, as shown in Eqs. (18) and (19) [45]:

$$O_{s1} = r_1 cP_1 + (1 - r_1 c)P_2 \tag{18}$$

$$O_{s2} = (1 - r_1 c)P_1 + r_1 cP_2 \tag{19}$$

where, P_1 and P_2 are parent one and two, O_{s1} and O_{s2} are offspring one and two, r_1 is a random number, and c is crossover fraction. In order to avoid any kind of diversity in population, operator shown in Eq. (20) is applied [45]:

$$O_s = O_s + \sigma\left(1 - \frac{sG_i}{G_m}\right) r_2 (u_b - l_b) \tag{20}$$

where, r_2 is random number, σ is standard deviation of random number, s is a scalar number that reduces the ratio of mutation, G_i is the current number of individuals, G_m is the maximum allowable number of individuals, u_b and l_b are upper bound and lower bound of the main optimization problem.

Finally, the members of the next generation are selected based on binary tournament selection method, as shown in Eq. (21) [45]:

$$dc_j = \sum_{v=1}^{V} \frac{f_v^{j_{j+1}} - f_v^{j_{j-1}}}{f_v^{\max} - f_v^{\min}} \tag{21}$$

where, dc_j is the crowding distance of j^{th} individual, V is the number of fitness functions, and f_v is the v^{th} fitness function.

The algorithm goes on until the stoppage criteria are met to terminate the program. The common stoppage criteria are maximum number of iterations, minimum changes of objective functions with respect to previous iteration, and maximum number of objective function evaluation. A general flowchart of NSGA II is shown in Fig. 4. One of the reasons behind the selection of the NSGA II is that it maintains the diverse set of solutions to guarantee that the resulted Pareto front covers the whole domain and not clustered in specific regions for the objective space. The non-dominated sorting is very practical for efficiently exploration of the Pareto front based on the relationships that could avoid the preserving non-dominated solutions. Also, the convergence speed of this algorithm is pretty much higher compared to other multi-objective algorithms. In terms of increased number of objective functions NSGA II performs excellent comparing to other multi-objective algorithms, which >2–3 objective function could endanger their convergence. Finally, the algorithm uses elitism, allowing the best solutions to survive across generations, thereby ensuring that the best solutions are not lost. Moreover, it employs tournament selection techniques to choose the most suitable solutions for reproduction and maintaining diversity. GA algorithms are always converged to optimal point and never stick in local optimal [46].

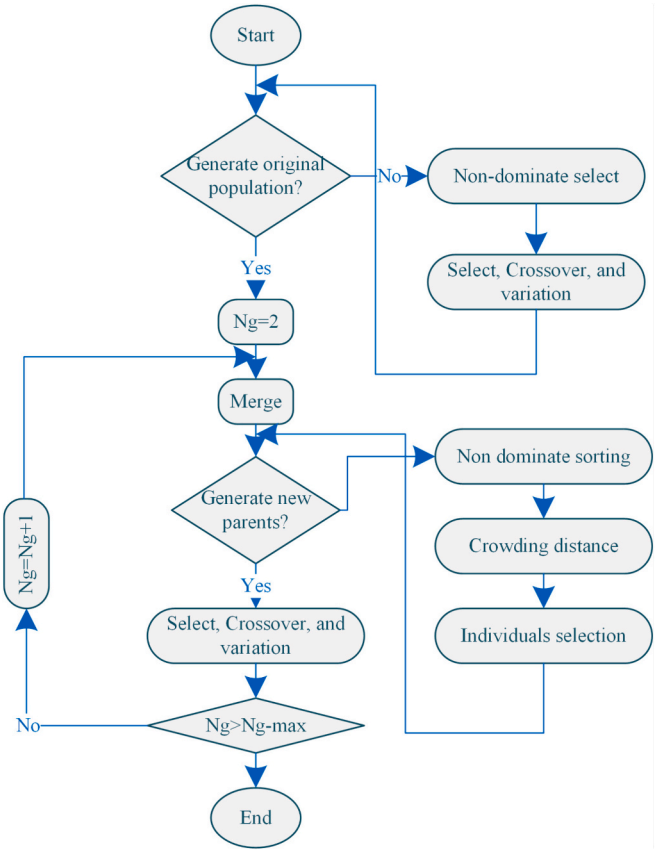

Fig. 4. A general flowchart of NSGA II implementation procedure.

In this paper, four objective functions are considered simultaneously to maximize the volumetric energy density, minimize the weight of SMES's conductor, minimize the cooling cost of SMES, and to minimize the maximum applied stress to the HTS tapes in the coils. Eq. (22) shows the objective functions in this paper while upper and lower limits of variables are shown in Eq. (23). These wide ranges of lower and upper bounds demonstrate the capability and robustness of our optimization algorithm in finding the absolute minimum and maximum, rather than merely identifying local optima. This stands in contrast to other references in the literature, where the search domain has been restricted to a narrow range to aid those optimization algorithms in locating the absolute optima. Our approach is particularly practical in the manufacturing and design of HTS devices, where designers and manufacturers often lack initial constraints on the possible values for a feasible design. By employing a broader search domain, our algorithm provides a more comprehensive exploration of potential solutions, ensuring that the resulting designs are not limited by initial assumptions. This flexibility is crucial in the field of HTS device development, where innovation and adaptation to new discoveries are essential. Therefore, our methodology not only enhances the likelihood of achieving optimal designs but also aligns with the dynamic and evolving nature of HTS technology. Also, it should be mentioned that the ranges shown in Eq. (23) have been chosen based on [33].

$$miny = min\left(\frac{1}{ED}, Weight, C_{cool}, \sigma_{max}\right) \tag{22}$$

$$\begin{aligned} 1.25\,mm &\le d_t \le 10.25\,mm \\ 14.1\,mm &\le d_p \le 24.1\,mm \\ 2 &\le N_t \le 976 \\ 2 &\le N_p \le 177 \\ 0.03\,m &\le R_{in} \le 1.25\,m \end{aligned} \tag{23}$$

In this study, the hyperparameters tabulated in Table 1, have been considered for NSGA II, since they resulted in best optimization results.

4. Results and discussion

To design the SMES, a Gadolinium Barium Copper Oxide (GdBCO) tape is used. The most important properties of this HTS tape are tabulated in Table 2.

4.1. Validation of SMES design model

The very first step is to validate the design formulae and electromagnetic model used in this paper with respect to the results of reference [33]. In [33], the loading factor ($m = \frac{I_{op}}{I_c}$) is 1 which means the operational current is equal to critical current. Although this assumption could increase the energy density and total energy of SMES, it could endanger the safe operation of SMES. In [33], two cases have been reported which have different structures (such as different turn numbers, pancake numbers, distances between turns and pancakes, etc.) while their stored energy is constant. We compared results of [33] with those of produced by our model in this paper in Table 3. Based on the validation results presented in Table 3, the maximum relative difference between our developed model and the model reported by [33] for case A, is <1.1 %, while this number for the second case is also <1.1 %. It should be also mentioned that the presented model in [33] was also validated with respect to FEM-based models with a maximum absolute difference of <2 % that shows the high accuracy of our presented electromagnetic analytical model of SMES. In both cases of A and B, the energy of the SMES is about 2.8 MJ which makes them suitable for power system applications. However, their main difference is in their energy density where case A has 3.5 times higher energy density which originated in different number of turns and different number of PCs. On the other hand, in case A, the critical current is much more reduced, compared to case B. Finally, the length of superconducting wire in case A is about 13 % higher than the length of superconductor wire in case B.

It should be mentioned that Table 3 serves a single purpose, which is to validate the model used for optimizing the structure of the SMES unit. Once the main model is validated, the process of SMES optimization begins.

4.2. Multi-objective optimization results

This paper aimed to show the importance of considering multiple objective functions during the design optimization process of an SMES. Then, discussions would be made to show the importance of considering the right value of loading factor during such investigations.

Fig. 5 shows the Pareto front of a multi-objective optimization by considering energy density, cooling cost, weight, and maximum applied stress as four objectives simultaneously. The reported values for energy density in some cases are even 25 % to 30 % higher than values reported in [33], however, these cases are extremely heavy with a high cooling cost. This is since in [33] single objective optimization is used while in our research MOO is used which could hand us a more reasonable and practical solution. The points shown in Fig. 5 are all the mathematically feasible solutions and based on the requirements, constraints, and limitations of the grid where SMES is going to be implemented, one must choose the optimum result, known as physically feasible solution.

Based on limitations and requirements presented in [33], the aim is to design an SMES device with 2.5 MJ energy. This power range is of interest for grid stability and Uninterruptible Power Supply (UPS) applications in certain microgrid. Based on the identified application, the optimal design would be investigated. The target energy could be treated mathematically as an additional inequity constraint where energy of designed SMES could be 10 % higher/lower than target energy, 2.5 MJ.

Firstly, we considered the loading factor to be 1 and then performed the optimization. Under such circumstances and based on results reported in Table 4, the best solution is where the energy is about 2.37 MJ and energy density is about 374.95 kJ/kg. This means that a 15 % reduction in energy value of optimized structure and about 40 % reduction in energy density value compared to case A of reference [33]. This means that considering the proper type and numbers of objective functions could limit the number of feasible solutions. In other words, the results reported in [33] are very optimistic and in real world, energy and energy density would be reduced due to constraints that cooling system, heat load, stress, and economic concerns impose to the designed SMES.

Secondly, we studied how loading factor affects the feasible solutions for SMES design optimization. The loading factor is now considered to be 0.8 and then optimization is performed again. To compensate the impact of operating current reduction, number of turns, number of pancakes, and inner radius of coil are increased. This would hand us a 2.36 MJ SMES with energy density of 291.08 kJ/kg which is reduced compared with m = 1 due to the increased weight of SMES according to the increases in number of turns, pancakes, and inner radius. Thus, if m = 0.8, energy is again about 15 % reduced, comparing to ideal optimistic results reported in [33] while this value for energy density is about 54 % reduction. Now, we go even further and just consider 60 % of critical current for operational current that results in further increase in the number of turns, pancakes, and inner radius which have 39 turns, 1 pancake, and 30 cm (about 11.81 in.) more value comparing to loading factor equal to 0.8. Here, energy is 16 % reduced while energy density reduces further and about 58 %. When the loading factor is 0.4 and 0.2, energy density gets even worse which is reduced 67 % and 78 %, comparing to [33], respectively.

The reported results have two obvious takeaways, first point declares that design optimization of an SMES unit just based on one or two objectives is not somehow realistic and could not meet the requirements in

Table 1
Hyperparameters used in this study for design optimization of an SMES unit.

Hyperparameter	Value
Maximum number of iterations	1000
Population size	500
Crossover percentage	70 %
Mutation percentage	30 %
Mutation rate	0.05
Mutation step size	0.003

Table 2
Most important properties of HTS tape.

Property	Value	Unit
Width	12.1	mm
Thickness	0.15	mm
Stabilizer thickness (material)	30 (Copper)	μm (–)
Superconductor thickness (material)	1 (GdBC)	μm (–)
Substrate thickness (material)	60 (Hastelloy)	μm (–)
Silver thickness	0.1	μm
Maximum allowable stress	250	MPa
Critical current @ 77 K and 0 T	708	A
Index value @ 77 K and 0 T	25	–
c_1	50	–
c_2	0.2	–
c_3	0.65	–

Table 3
Model validation based on study conducted in [33].

Parameter	Results of our proposed method - case A	Results reported in [33] - case A	Relative error (%)	Results of our proposed method - case B	Results reported in [33] - case B	Relative error (%)
Energy (MJ)	2.76	2.79	−1.07	2.75	2.78	−1.07
Energy density (kJ/kg)	628.02	630	−0.31	177.67	178	−0.18
Inductance (H)	1455.5	1455.1	0.03	686.92	686.72	0.03
Ic (A)	61.60	61.04	−0.71	88.90	88.98	−0.18
Wire length (km) for a 12 mm wide HTS tape	195.39	195.39	0	173.36	173.35	0

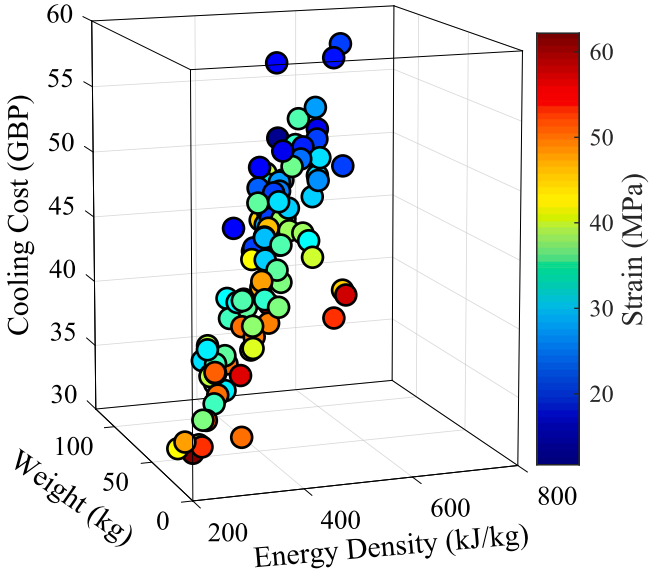

Fig. 5. Pareto front resulted by a multi-objective optimization of an MJ class SMES.

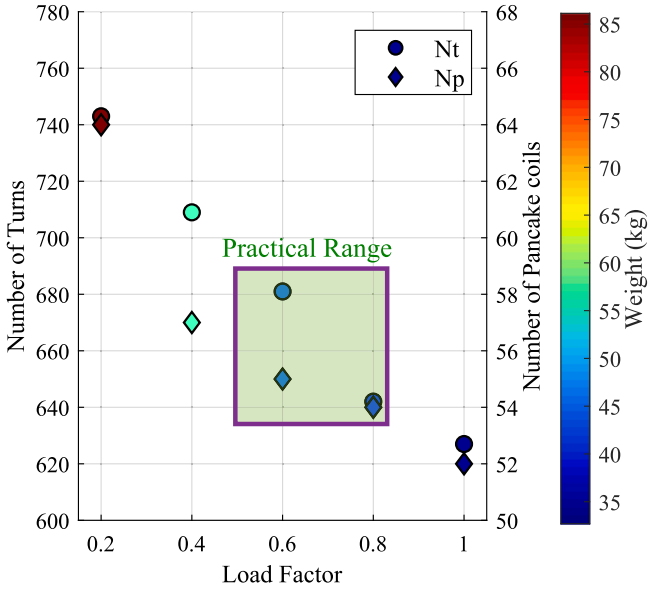

Fig. 6. Impact of loading factor on the optimum number of turns, number of pancake coils, and weight in SMES.

Table 4
Impact of different loading factors on optimum energy density and optimized structure.

Loading factor	m = 1	m = 0.8	m = 0.6	m = 0.4	m = 0.2
Energy density (kJ/kg)	374.95	**291.08**	**264.97**	205.02	136.82
Energy (MJ)	2.37	**2.36**	**2.35**	2.34	2.31
dt (mm)	1.43	**1.51**	**1.51**	1.51	1.63
dp (mm)	24.20	**24.5**	**24.5**	24.5	26.3
Nt	627	**642**	**681**	709	743
Np	52	**54**	**55**	57	64
Ic(B)	70.04	**76.11**	**79.77**	83.56	100.91
Rin (m)	0.36	**0.41**	**0.43**	0.44	0.45

real word for commercializing this device. The second point is about the impact of loading factor on the final and feasible solutions. The lower the loading factor gets, the energy density would be reduced which is due to the increase in number of turns, pancakes, and inner radius to reach the energy of SMES in range of 2.5 MJ.

4.3. Importance of considering different loading factors

Fig. 6 shows the impact of loading factor reduction on the structural parameters of the understudied SMES. As can be seen, the number of turns, number of pancake coils, and total weight of the coil are increased when loading factor is reduced. This is because when loading factor is decreased, less operating current could pass through HTS tapes. As a result, more turns and more coils are needed to deliver the demanded energy (around 2.5 MJ) and thus, the total weight of SMES is increased. As shown in Fig. 5, the number of turns for m = 0.6, is about 680 while this number for m = 0.8 is about 710 (about 4 % reduction) meanwhile the number of pancake coils are reduced about 5 %. This reduction in the number of turns and pancake coils results in 27 % reduction of SMES

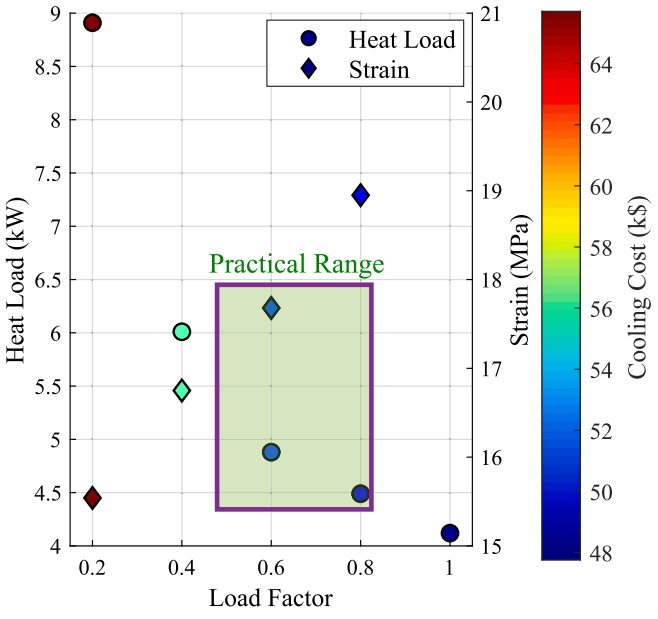

Fig. 7. Impact of loading factor on the optimum heat load, maximum strain, and cooling cost in SMES.

total weight. So, higher loading factor could reduce the total weight of SMES and its energy density. On the other hand, increasing the loading factor could generate hot spots in HTS tape, initiate weak points, and quenches and eventually results in coil burnout in SMES [47].

Fig. 7 depicts the impact of loading factor variations on heat load, maximum applied strain, and cooling cost of the designed SMES. As shown in this figure, the higher loading factor results in reduction of the total heat load imposed to the cooling system. This is because the loading factor increase results in the reduction of number of turns and the number of pancake coils. Due to this reduction, less heat is accumulated in coils and turns. For instance, when loading factor is 0.6, heat load is about 6.1 kW while this number for loading factor of 0.8 is about 4.5 kW which means a 25 % heat load reduction. On the other hand, 11 % of the cooling cost is also reduced by increasing the loading factor from 0.6 to 0.8. However, as discussed before, the increase in loading factor could increase the possibility of quenching in HTS tape. Thus, one may need to find a compromise between the considered value of loading factor, total heat load, cooling cost, and quench probability. Maximum applied strain is also another physical reason for quenching propagation through the length of HTS tapes. As shown in Fig. 6, when the loading factor increases, maximum applied strain to the HTS tapes is also increased. This approves our previous discussion that the loading factor increment could result in the increasing the probability of quenches.

4.4. Results comparison by PSO

In this section, the results of NSGA II-based optimization have been compared with results of Particle Swarm Optimization (PSO) algorithm. PSO is one of the most effective swarm-based optimizers that has been studied in literature for optimizing different systems and devices [48–51]. To compare the results of PSO with NSGA II algorithm, firstly we have changed the objective function as a summation of energy density, cooling cost, maximum strain, and weight. Then, hyper-parameters of the PSO has been set as, maximum iteration to be 1000, population size 500, inertia weight and its damping ratio are 0.7298 and 1, and personal/global learning coefficients are both 1.4962. Then, the optimization has been triggered and results of each simulation have been shown in Table 5. According to this table, when loading factor of SMES unit is 1, the optimized ED by PSO is 250 kJ/kg which is equal to 33 % reduction of the ED optimized by NSGA II. Also, amount of optimized energy by PSO has been 49 % reduced, compared to optimized results of NSGA II. Design of SMES has been also optimized by PSO, for loading factor of 0.6. In this case, optimized energy density has faced 77 % reduction in energy density and 50 % reduction in maximum energy. As seen in this table, in both cases optimized by PSO inner radius has been optimized to have 1.25-meter value and distance between turns is about 10 mm which is originated in fact that PSO tries to avoid strong magnetic field generation to stop the massive critical current reduction. This would lead to maximizing the energy generated by the superconducting coil. However, since the coil has become bulkier, the energy density has would be reduced. This could be translated as local optima points for this problem.

Table 5
Impact of different loading factors on optimum energy density and optimized structure.

Loading factor	m = 1		m = 0.6	
Optimization algorithm	NSGA II	PSO	NSGA II	PSO
Energy density (kJ/kg)	374.95	250.93	264.97	59.48
Energy (MJ)	2.37	1.21	2.35	1.16
dt (mm)	1.43	10.03	1.51	10.02
dp (mm)	24.20	14.11	24.5	14.11
Nt	627	281	681	189
Np	52	50	55	50
Ic(B)	70.04	156.92	79.77	156.77
Rin (m)	0.36	1.25	0.43	1.25

4.5. Loading factor optimization

In this section, the loading factor has been added to the NSGA II algorithm as an optimization variable to see how it can contribute to the optimization of SMES design. The inclusion of the loading factor is intended to explore its impact on the overall performance and efficiency of the design. Five solutions fall within the range of our desired energy, approximately 2.5 MJ, as presented in Table 6. These solutions provide a diverse set of parameters that help understand the relationship between the loading factor and the SMES design.

As shown in Table 6, the range of distance between turns is approximately 1 mm, while the range of distance between coils varies among different solutions. This variation indicates the flexibility of the design in accommodating different configurations while still achieving the desired energy output. The optimized value of the loading factor is either near 0.4 or near 0.6, and far from 1. This is because, although the energy increases by considering the loading factor as 1, the heat load rapidly increases, results in extremely high cooling expenses. Managing these expenses is crucial for maintaining the overall cost-effectiveness of the design.

It should be mentioned that in the case of higher loading factors, the maximum strain applied to the cable increases compared to lower loading factors. This is due to two main reasons; first, the high amount of current induces a high level of magnetic field in the HTS tapes, which causes an increase in maximum electromagnetic forces. This magnetic field interacts with the material properties of the tapes, leading to mechanical stress. Secondly, in these cases with a higher loading factor, the number of turns is greater than in low loading factor solutions. This increase in the number of turns intensifies the maximum magnetic field of the SMES unit, which further contributes to higher strain. Understanding these effects is important for designing a robust and reliable SMES system that can operate efficiently under various conditions.

For the sake of the validation of our model used for electromagnetic calculations of the designed SMES, Fig. 8 has been presented. The aim of this figure is to validate the results of analytical approach for magnetic field calculations with Finite Element Method (FEM). The FEM-based modelling has been conducted based on the procedure proposed in [33] for HTS coil electromagnetic modelling and the results have been calculated for solution 1 shown in Table 6. Fig. 8(a) illustrates the radial magnetic field of studied HTS coil, as shown in this figure radial magnetic field calculated by analytical method is in good coordination with radial magnetic field calculated by FEM-based model. Fig. 8(b) demonstrates the axial magnetic field and compares the results of analytical and FEM-based models. As shown in this figure, axial magnetic field calculated by analytical model is in good coordination with FEM-based models. It should be noted that the results of FEM and analytical model have been shown in Fig. 8, based on the values of magnetic field

Table 6
Results of optimization considering the loading factor, the possible solutions.

Optimum solutions	Solution 1	Solution 2	Solution 3	Solution 4	Solution 5
dt (mm)	1.1	1.1	1.0	1.2	1.8
dp (mm)	18.5	16.5	16.3	20.6	23.9
Rin (mm)	162.5	215.2	171.3	203.5	621.8
Np	42	62	43	41	64
Nt	490	596	490	477	854
Loading factor	0.4739	0.7274	0.4652	0.3966	0.6827
Energy density (kJ/kg)	170.26	329.35	269.98	240.89	304.08
Energy (MJ)	2.56	2.47	2.68	2.33	2.45
Weight (kg)	65.77	35.78	40.77	40.88	37.34
Cooling cost (GBP)	55.83	50.55	52.19	52.85	47.42
Maximum strain (MPa)	2.12	18.42	7.71	5.81	14.70
Ic(B)	131.93	92.71	93.07	96.94	102.81

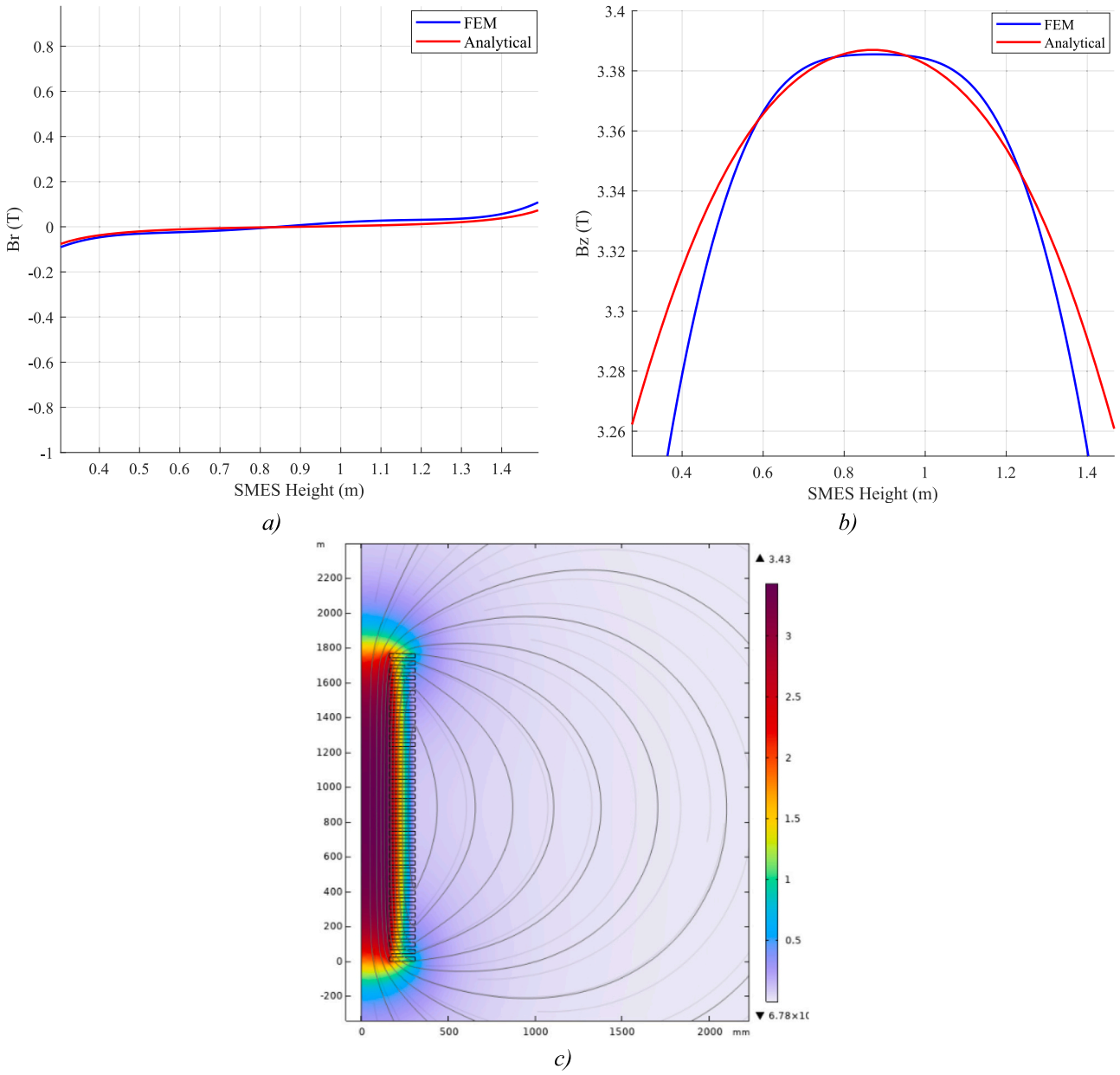

Fig. 8. Comparison of FEM-based results with the results of analytical approach, a) radial magnetic field comparison, b) axial magnetic field comparison, c) total magnetic field distribution.

components in inner edge of the HTS coil. Total magnetic field of HTS coil is also depicted in Fig. 8(c).

4.6. Further discussions on the results

So far, we have discussed the impact of loading factor and different objectives during design optimization of a 2.5 MJ-class SMES. In this subsection, we would generalize some of the results for any class of SMES for different applications. The very first lesson is about the importance of considering multiple goals/targets/objectives during designing an SMES unit. In this regard, it is crucial to take the electromagnetic, economic, mechanical, and structural objectives into account. For instance, when one designs an SMES just based on maximizing the total energy of the device, this may lead to an SMES with massive weight, and low energy density which is practically unreal or very expensive to fabricate and operate. On the other hand, one could state that instead of considering total energy as objective, energy density could be considered as design objective. Although, this may be a solution to the weight problem, the designed SMES could have a high heat load, high cooling cost, or even faces quenches due to high value of stress. Thus, these terms must be included in design optimization of SMES to avoid previously stated problems and to have an SMES unit with practical design parameters.

Secondly, the loading factor considered during design process of SMES plays a crucial role to reduce the probability of quenches through the whole length of HTS tape and to achieve the highest possible energy density by reducing the mass of SMES and reducing the price of SMES. The loading factor has a direct impact on total ownership cost of SMES unit. The higher loading factor means that we may need less turns and less pancake coils and thus lower purchasing cost of HTS tape. On the other hand, the increase in the loading factor could reduce the cooling cost of the SMES unit. So, one may declare that we could consider this value to be 1. However, considering this value for loading factor increases the probability of quenches and because of this HTS tapes may

suffer burnouts that results in failures of SMES. Thus, the loading factor must be selected based on multiple factors such as operating temperature of SMES, the application of SMES, the structural properties of HTS tape, and the capacity of cooling system.

Finally, it should be noted that there are several challenges and benefits associated with the deployment of SMES for actual large-scale multi-machine systems. One of them is the cost of superconducting materials for such large-scale applications, as many turns and pancake coils are needed. Additionally, maintaining the cryogenic temperatures involves significant expenses and complex infrastructure. Integrating SMES units with existing power grids and multi-machine systems requires sophisticated engineering to ensure compatibility. Developing advanced control systems to manage the fast response and high-power discharge of SMES is another challenge. Moreover, regular maintenance is needed to ensure the superconducting state is preserved, which can be challenging. Another challenge is the degradation of superconductors over time and overcurrent, which affects the longevity and reliability of the SMES system. However, by addressing all these challenges, SMES units could add fast response time, instantaneous power delivery, reliable frequency regulation, voltage support, power quality improvement, and the capability to mitigate fluctuations to the power system.

5. Conclusion

Considering the increasing demand for electrical energy and the rising penetration of renewable energy sources, the interest in devices capable of storing electrical energy has grown significantly. Among the most promising technologies for energy storage are Superconducting Magnetic Energy Storage (SMES) units. SMES devices in the MJ class, offering hundreds of kilowatts of capacity, present outstanding solutions for microgrids, where the instability caused by the uncertainty of renewable energy resources needs to be addressed. These SMES devices offer low weight, high energy density, and minimal losses compared to other alternatives. However, their design presents some challenges and requires consideration of multiple factors during the design process. To tackle this, the current research utilizes a multi-objective algorithm, known as Non-dominated Sorting Genetic Algorithm II (NSGA II), to optimally design the SMES unit and explore the impact of different loading factors for High Temperature Superconducting (HTS) tapes. The most important findings of this paper can be summarized as follows: Using a multi-objective optimization method to design an SMES unit leads to a wide range of possible solutions, forming the Pareto front. The loading factor, which represents the ratio of operational current to critical current, plays a crucial role in achieving feasible solutions. For an optimal and feasible solution with a loading factor of 0.6, the number of turns is approximately 680. However, if the loading factor is increased to 0.8, the number of turns decreases to 710, representing a reduction of about 4 %. Similarly, the number of pancake coils is reduced by approximately 5 % when changing the loading factor from 0.6 to 0.8. This reduction in the number of turns and pancake coils results in a 27 % reduction in the total weight of the SMES unit. When the loading factor is set to 0.6, the heat load is about 6.1 kW, while for a loading factor of 0.8, it reduces to approximately 4.5 kW. By changing the loading factor from 0.6 to 0.8, there is an 11 % reduction in the cooling cost. These findings demonstrate the significance of considering the loading factor and how it can influence the design and performance of the SMES unit. After doing this, results of optimization by NSGA II have been compared by the results of optimization by using Particle Swarm Optimization algorithm. The results have shown that NSGA II could perform better by designing an SMES unit with higher energy, higher energy density, and lower weight. Finally, the loading factor itself has been considered as an optimization variable. By doing this, 5 different solutions have been proposed by NSGA II with energy range of 2 MJ while the loading factor had a value between 0.39 and 0.72, as optimized value. Finally, the Finite Element Method-based simulations have used to validate the electromagnetic results.

CRediT authorship contribution statement

Alireza Sadeghi: Writing – original draft, Visualization, Software, Methodology, Investigation, Formal analysis, Data curation, Conceptualization. **Antonio Morandi:** Writing – review & editing, Validation, Supervision, Methodology, Investigation, Formal analysis, Conceptualization. **Mohammad Yazdani-Asrami:** Writing – review & editing, Validation, Supervision, Resources, Project administration, Methodology, Investigation, Funding acquisition, Formal analysis, Conceptualization.

Declaration of competing interest

The authors declare that they have no known competing financial interests or personal relationships that could have appeared to influence the work reported in this paper.

Data availability

Data will be made available on request.

Acknowledgments

References

[1] A.Q. Al-Shetwi, M.A. Hannan, K.P. Jern, M. Mansur, T.M.I. Mahlia, Grid-connected renewable energy sources: review of the recent integration requirements and control methods, J. Clean. Prod. 253 (2020) 119831.
[2] G.G. Farivar, et al., Grid-connected energy storage systems: state-of-the-art and emerging technologies, Proc. IEEE vol. Early Acce (2022) 1–24.
[3] J. Gómez, B. Pérez, P. Suárez, A. Álvarez, B. Rivera, Theoretical and experimental studies of SMES con-figurations for design optimization, IEEE Trans. Appl. Supercond. 31 (5) (2021) 1–5.
[4] C. Gandolfi, R. Chiumeo, D. Raggini, R. Faranda, A. Morandi, C. Ferdeghini, Study of a universal power SMES compensator for LV distribution grid, in: 2018 AEIT International Annual Conference, 2018, pp. 1–6.
[5] A. Morandi, M. Fabbri, B. Gholizad, F. Grilli, F. Sirois, V.M.R. Zermeño, Design and comparison of a 1-MW/5-s HTS SMES with toroidal and solenoidal geometry, IEEE Trans. Appl. Supercond. 26 (4) (2016) 1–6.
[6] A. Morandi, et al., Calculation of AC losses in a 500 kJ/200 kW multifilamentary MgB2 SMES coil, Energies (Basel) 16 (4) (2023) 1596.
[7] M. Yazdani-Asrami, A. Sadeghi, S. Seyyedbarzegar, W. Song, DC electro-magneto-mechanical characterisation of 2G HTS tapes for superconducting cable in magnet system using artificial neural networks, IEEE Trans. Appl. Supercond. Early Acce (2022) 1–11.
[8] A. Morandi, L. Trevisani, F. Negrini, P.L. Ribani, M. Fabbri, Feasibility of superconducting magnetic energy storage on board of ground vehicles with present state-of-the-art Superconductors, IEEE Trans. Appl. Supercond. 22 (2) (2012) 5700106, https://doi.org/10.1109/TASC.2011.2177266.
[9] V.S.V. G, S. Madichetty, Application of superconducting magnetic energy storage in electrical power and energy systems: a review, Int. J. Energy Res. 42 (2) (2018) 358–368, https://doi.org/10.1002/er.3773.
[10] M. Yazdani-Asrami, W. Song, A. Morandi, G. De Carne, J. Murta-Pina, A. Pronto, Roadmap on artificial intelligence and big data techniques for superconductivity, Supercond. Sci. Technol. Early Acce (2023).
[11] A. Kumar, J.V.M.L. Jeyan, A. Agarwal, Numerical analysis on 10 MJ solenoidal high temperature superconducting magnetic energy storage system to evaluate magnetic flux and Lorentz force distribution, Phys. C 558 (Mar. 2019) 17–24, https://doi.org/10.1016/j.physc.2019.01.001.
[12] Z. Zhao, Y. Wang, Y. Gao, Z. Yang, Z. Li, W. Pi, Mechanical characterization of a 10-MJ HTS SMES magnet wound by quasi-isotropic strands and directly stacked tape conductors, Superconductivity 5 (Mar. 2023) 100042, https://doi.org/10.1016/j.supcon.2023.100042.
[13] A. Kumar, R. Kaur, Electromagnetic Analysis of 1MJ Class of High Temperature Superconducting Magnetic Energy Storage (SMES) Coil to be Used in Power Applications, 2018, p. 050003, https://doi.org/10.1063/1.5050751.
[14] C.A. Borghi, M. Fabbri, P.L. Ribani, Design optimization of a microsuperconducting magnetic energy storage system, IEEE Trans. Appl. Supercond. 35 (5) (1999) 4275–4284.
[15] P. Tixador, et al., SMES optimization for high energy densities, IEEE Trans. Appl. Supercond. 22 (3) (2012) 5700704.

[16] J. Ciceron, A. Badel, P. Tixador, F. Forest, Design considerations for high-energy density SMES, IEEE Trans. Appl. Supercond. 27 (4) (2017) 1–5.
[17] X. Yu, M. Song, Optimization design of SMES solenoids considering the coil volume and the magnet volume, IEEE Trans. Appl. Supercond. 18 (2) (2008) 1517–1520, https://doi.org/10.1109/TASC.2008.921968.
[18] W.S. Kim, et al., Design of HTS magnets for a 600 kJ SMES, IEEE Trans. Appl. Supercond. 16 (2) (2006) 620–623, https://doi.org/10.1109/TASC.2005.864244.
[19] S.Y. Lee, et al., Optimal design of HTS magnets for a modular toroid-type 2.5 MJ SMES using multi-grouped particle swarm optimization, Phys. C: Supercond. Applic. 469 (15–20) (2009) 1789–1793, https://doi.org/10.1016/j.physc.2009.05.149.
[20] S. Fang, G. Chao, H. Lin, A method to improve volume energy density for HTS coil, IEEE Trans. Appl. Supercond. 29 (2) (2019) 1–4, https://doi.org/10.1109/TASC.2018.2889618.
[21] Y. Xu, et al., A study on the design and comparison of 1–100-MJ-class SMES magnet with different coil configurations, IEEE Trans. Appl. Supercond. 27 (5) (2017), https://doi.org/10.1109/TASC.2017.2707669.
[22] A.H. Moghadasi, H. Heydari, M. Farhadi, Pareto optimality for the design of smes solenoid coils verified by magnetic field analysis, IEEE Trans. Appl. Supercond. 21 (1) (2011) 13–20, https://doi.org/10.1109/TASC.2010.2089791.
[23] A. Kumar, A. Agrawal, J.M.L. Jeyan, A numerical model comprising the effect of number of turns on AC losses in 2G HTS coated conductor at 77K using H-formulations, in: In *2019 IEEE 2nd International Conference on Power and Energy Applications (ICPEA)*, IEEE, Apr. 2019, pp. 115–118, https://doi.org/10.1109/ICPEA.2019.8818528.
[24] Z. Wang, et al., AC loss analysis of a hybrid HTS magnet for SMES based on <italic>H</italic>-formulation, IEEE Trans. Appl. Supercond. 27 (4) (Jun. 2017) 1–5, https://doi.org/10.1109/TASC.2016.2646480.
[25] Y. Xu, et al., Distribution of AC loss in a HTS magnet for SMES with different operating conditions, Phys. C Supercond. 494 (Nov. 2013) 213–216, https://doi.org/10.1016/j.physc.2013.04.079.
[26] C. Hernando, J. Munilla, L. García-Tabarés, G. Pedraz, Optimization of high power SMES for naval applications, IEEE Trans. Appl. Supercond. 33 (5) (Aug. 2023) 1–5, https://doi.org/10.1109/TASC.2023.3250169.
[27] A. Anand, A.S. Gour, T.S. Datta, V.V. Rao, Study on HTS SMES coil for optimized dimensions, IEEE Trans. Appl. Supercond. 33 (7) (Oct. 2023) 1–11, https://doi.org/10.1109/TASC.2023.3289092.
[28] A. Anand, A.S. Gour, T.S. Datta, V.V. Rao, 50 kJ SMES magnet design optimization using real coded genetic algorithm, IOP Conf. Ser. Mater. Sci. Eng. 1240 (1) (May 2022) 012137, https://doi.org/10.1088/1757-899X/1240/1/012137.
[29] Zhao Yuan, Yu Xinjie, Pareto competition based evolution strategy for two-objective optimization design of SMES solenoids, IEEE Trans. Appl. Supercond. 18 (2) (Jun. 2008) 1513–1516, https://doi.org/10.1109/TASC.2008.921971.
[30] M. Khosraviani, M. Jahanshahi, M. Farahani, A.R.Z. Bidaki, Load–frequency control using multi-objective genetic algorithm and hybrid sliding mode control-based SMES, Int. J. Fuzzy Syst. 20 (1) (Jan. 2018) 280–294, https://doi.org/10.1007/s40815-017-0332-z.
[31] A.H.K. Asadi, A. Jahangiri, M. Zand, M. Eskandari, M.A. Nasab, H. Meyar-Naimi, Optimal design of high density HTS-SMES step-shaped cross-sectional solenoid to mechanical stress reduction, in: In *2022 International Conference on Protection and Automation of Power Systems (IPAPS)*, IEEE, Jan. 2022, pp. 1–6, https://doi.org/10.1109/IPAPS55380.2022.9763198.
[32] A.H. Moghadasi, H. Heydari, M. Farhadi, Pareto optimality for the design of SMES solenoid coils verified by magnetic field analysis, IEEE Trans. Appl. Supercond. 21 (1) (Feb. 2011) 13–20, https://doi.org/10.1109/TASC.2010.2089791.
[33] P.R. Raut, H.J. Bahirat, M.D. Atrey, Analytical approach for optimal HTS solenoid design, IEEE Trans. Appl. Supercond. 31 (2) (2021) 1–9, https://doi.org/10.1109/TASC.2020.3038531.
[34] J.T. Conway, Trigonometric integrals for the magnetic field of the coil of rectangular cross section, IEEE Trans. Magn. 42 (5) (2006) 1538–1548, https://doi.org/10.1109/TMAG.2006.871084.
[35] A. Morandi, B. Gholizad, M. Fabbri, Design and performance of a 1 MW-5 s high temperature superconductor magnetic energy storage system, Supercond. Sci. Technol. 29 (1) (2015) 015014, https://doi.org/10.1088/0953-2048/29/1/015014.
[36] M. Abdel-Salam, A. Elnozahy, M. Elgamal, Minimum power loss based design of SMES as influenced by coil material, J. Energy Storage 30 (2020) 101461, https://doi.org/10.1016/j.est.2020.101461.
[37] S.S. Kalsi, Applications of High Temperature Superconductors to Electric Power Equipment, John Wiley & Sons, 2011.
[38] M.N. Wilson, Superconducting Magnets, Oxford University Press, 1987.
[39] X. Zhou, et al., Cost estimation models of MJ class HTS superconducting magnetic energy storage magnets, IEEE Trans. Appl. Supercond. 28 (4) (2018) 1–5, https://doi.org/10.1109/TASC.2018.2821363.
[40] A. Sadeghi, M. Yazdani-Asrami, Multi-objective optimization for improving weight and fault characteristics of a DC HTS cable in cryo-electric aircraft, Aerospace 9 (12) (2022) 753.
[41] N. Gunantara, Q. Ai, A review of multi-objective optimization: methods and its applications, Cogent. Eng. 5 (1) (2018) 1502242.
[42] H.A. Abbass, R. Sarker, C. Newton, PDE: a Pareto-frontier differential evolution approach for multi-objective optimization problems, in: Proceedings of the 2001 Congress on Evolutionary Computation (IEEE Cat. No.01TH8546), 2001, pp. 971–978.
[43] M. Ehrgott, Multicriteria Optimization, Springer Science & Business Media, 2005.
[44] K. Deb, A. Pratap, S. Agarwal, T. Meyarivan, A fast and elitist multiobjective genetic algorithm: NSGA-II, IEEE Trans. Evol. Comput. 6 (2) (2002) 182–197.
[45] A. Palaparthi, T. Riede, I.R. Titze, Combining multiobjective optimization and cluster analysis to study vocal fold functional morphology, I.E.E.E. Trans. Biomed. Eng. 61 (7) (2014) 2199–2208.
[46] H. Ma, Y. Zhang, S. Sun, T. Liu, Y. Shan, A comprehensive survey on NSGA-II for multi-objective optimization and applications, Artif. Intell. Rev. 56 (12) (Dec. 2023) 15217–15270, https://doi.org/10.1007/s10462-023-10526-z.
[47] A. Sadeghi, Z. Xu, W. Song, M. Yazdani-Asrami, Intelligent probability estimation of quenches caused by weak points in high temperature superconducting tapes, Energies (Basel) E. A (2023).
[48] J. Nayak, H. Swapnarekha, B. Naik, G. Dhiman, S. Vimal, 25 years of particle swarm optimization: flourishing voyage of two decades, Arch. Comput. Methods Eng. 30 (3) (Apr. 2023) 1663–1725, https://doi.org/10.1007/s11831-022-09849-x.
[49] Mei-Ping Song and Guo-Chang Gu, "Research on particle swarm optimization: a review," in *Proceedings of 2004 International Conference on Machine Learning and Cybernetics (IEEE Cat. No.04EX826)*, IEEE, pp. 2236–2241. doi:https://doi.org/10.1109/ICMLC.2004.1382171.
[50] J. Kennedy and R. Eberhart, "Particle swarm optimization," in *Proceedings of ICNN'95- International Conference on Neural Networks*, IEEE, pp. 1942–1948. doi: https://doi.org/10.1109/ICNN.1995.488968.
[51] D. Wang, D. Tan, L. Liu, Particle swarm optimization algorithm: an overview, Soft. Comput. 22 (2) (Jan. 2018) 387–408, https://doi.org/10.1007/s00500-016-2474-6.